Imaging the deep carbon stocks with complex electrical conductivity

Adrián Flores Orozco[1], Jakob Gallistl[1,2], Benjamin S. Gilfedder[3], Timea Katona[1], Sven Frei[4], Peter Strauss[5], and Gunter Blöschl[6],

[1]Department of Geodesy and Geoinformation, TU Wien, Vienna, 1040, Austria
[2]Near Surface Geophysics, GeoSphere Austria, Vienna, 1190, Austria
[3] Chair of Hydrology, Faculty of Regional and Environmental Sciences, University of Trier, Trier, Germany.
4Department of Environmental Science, Wageningen University & Research, Wageningen, 9101, The Netherlands
[5]Institute for Land and Water Management Research, Federal Agency for Water Management, Scharfling, 5310, Austria
[6]Institute of Hydraulic Engineering and Water Resources Management, TU Wien, Vienna, 1040, Austria

Correspondence to: Adrian Flores Orozco (Adrian.flores-orozco@geo.tuwien.ac.at)

Abstract. Mapping of soil organic carbon (SOC) is usually restricted to the top 100 cm of soils due to the limited penetration depth of standard soil sampling methods. This has resulted in current models underestimating SOC due to the unexplored deep carbon stocks. Moreover, standard methods only offer punctual data relying on interpolation to investigate extensive areas. We demonstrate here that subsurface 2D images of the complex electrical conductivity (CC) can delineate the presence and geometry of SOC reaching a depth of a few tens of meters below the surface. We show that an increase in the polarization effect at low frequencies (< 5 Hz) is linearly related to high concentrations of SOC. We present measurements from a catchment with silty loam soils, where the geometry of a deep carbon stock (between 4 and 6 m depth) was identified by CC images, and validated through laboratory analysis of soil samples.

1 Introduction

Soils are the largest terrestrial reservoir of organic carbon with the potential for long-term carbon storage (e.g., Panagos et al., 2013). Estimating soil organic carbon content (SOC) and inventories is therefore critically important for realistically evaluating the global C balance and changes in this budget due to human activities (Ganzenmüller et al., 2025). Current methods primarily estimate SOC for the topsoil (0 to 100 cm depth), as they contain the largest concentrations of SOC (e.g., Harrison et al. 2011; Yost and Hartemink, 2020). However, topsoils have limited potential to sequester further carbon, and it can be rapidly processed and released to the atmosphere due to high rates of microbial respiration and soil disturbances (Button et al., 2022 and references therein). Mapping of SOC in deep soils (> 100 cm) has been seldom addressed due to the enormous costs required for detailed deep drilling over large areas, and analysis of the large number of samples this implies (Harrison et al. 2011; Yost and Hartemink, 2020). Based on the analysis of boreholes reaching 37 m depth, Harper and Tibbett (2013) reported an increase in SOC storage at deep soils correlated with rainfall and following reforestation. Likewise, deep carbon stocks in permafrost soils are poorly understood with estimations made from the interpolation of sparse data (e.g., Tarnocai et al., 2009; Strauss, et al., 2013; Walter Anthony, 2018); although the thawing of such soils has a direct impact on climate change. Random

drilling is ineffective for sampling of deep SOC layers, especially when only a limited number of cores can be taken. Thus, any investigation of deep carbon stocks requires prior information for designing survey sampling strategies.

Geophysical methods permit the collection of quasi-continuous information about subsurface properties in a non-invasive manner. Among them, electrical methods have proved their potential to resolve geological, hydraulic and chemical properties of the soil (see Kemna et al., 2012; Kessouri et al., 2019; Binley et al., 2015). Electrical methods, such as the electrical resistivity tomography (ERT) and associated complex conductivity (CC), resolve subsurface electrical properties at low frequencies (< 1 kHz). The methods are based on an electrode pair used to inject a current into the ground, while other electrode pairs measure the resulting electrical field (see Appendix 5.2 and references therein). Current flow in the soils takes place along the fluid filling the pores (electrolytic conduction) and at the electrical double layer (EDL) formed at the grain fluid interface (surface conductivity). Thus, it is controlled by porosity, saturation, the conductivity of the pore water as well as surface charge, soil surface area and cation exchange capacity (CEC) of the solid phase. Additionally, current flow causes the polarization of charges in the EDL, resulting in a secondary electrical field observed after switching off the current. The conductive and capacitive properties of soils can be expressed by the complex conductivity (σ^*), consisting of a real (σ', representing the conduction or energy loss) and an imaginary (σ'', representing the capacitance or energy storage) components. The highest conduction and polarization effect can be observed in presence of electronic conductors such as sulphide minerals; thus, rendering the CC method optimal for mining applications (Seigel et al., 2017 for a review). Based on this, the CC has been used to monitor the precipitation of iron sulphides (FeS) accompanying the stimulation of iron reducing bacteria in laboratory experiments (Williams et al., 2005; Ntarlagiannis et al., 2005) and at the field-scale in the bioremediation of uranium-contaminated aquifer (Flores Orozco et al., 2011; 2013). The CC measurements have also been conducted at the floodplain-scale to map naturally reduced zones, due to the stimulation of iron-reducing microbes taking place in areas with high concentrations of organic matter in soils (Wainwright et al., 2015).

In absence of electronic conductors, the polarization of an alternating current injected into the soil (i.e., soil capacitance) is mainly controlled by the properties of the fluid-grain interface. Accordingly, CC has been largely used to delineate immiscible organic contaminants (e.g., Flores Orozco et al., 2012a; Schwartz and Furman, 2012; Johansson et al., 2015). Moreover, laboratory experiments have demonstrated the sensitivity of CC to the adsorption of organic matter (OM) to mineral grain surfaces (Schwartz et al., 2014; Mellage et al., 2022) due to the formation of organo-mineral complexes (Schwartz and Furman, 2014); while Strobel et al. (2023) reported high σ'' values (around 50 Hz) in samples taken from degraded peatlands. Pehstani et al. (2025) investigated the adsorption of pentaglycine onto ferrihydrite-coated sand and argue that the increase in both conductivity (σ') and polarization (σ'') is due to the interaction between the grain surface and organic functional groups (e.g., carboxyl and amine). These results demonstrate the possibility of the CC method to investigate the interaction between organic compounds and porous media.

To date only few studies have applied the CC method at the field scale to investigate changes in SOC. Flores Orozco et al. (2020) revealed anomalous regions characterized by high σ' and σ'' in waste containing high concentrations of total organic carbon (TOC) measured in leachates; whereas surveys conducted in peatlands have also revealed an increase in the polarization

response with increasing the SOC (McAnallen et al., 2018; Katona et al., 2021); although Ponziani et al., (2012) reported a decrease in σ'' with increasing peat humification. However, to date, the CC has not been applied to investigate large scale variations in SOC in mineral soils.

Deforestation, reforestation, land use and climate change have a direct impact on the dynamics of SOC, yet the response of deep (>1 m) carbon pools remains poorly understood. To fill this knowledge gap, this study aims at evaluating the potential of CC images for mapping anomalies in SOC concentrations at varying depths in loamy soils. This study focusses on deep investigations (> 1 m), which are rarely investigated in soil surveys, yet may be critical for the computation of more realistic organic carbon budgets as suggested by Harper and Tibbett (2013) among others. All data sets were collected at the HOAL (se Appendix 5.3), located in Petzenkirchen (Austria), which is a 66 ha research catchment dedicated to understanding water-related flow and transport processes involving sediments, nutrients and microbes in small catchments (Blöschl et al., 2016).

2 Results

2.1 The electrical properties of the HOAL – imaging results at 1Hz

Figure 1 shows the CC imaging results obtained for the measurements along the exploration line E1. Here two layers can be visually identified: (1) on the top the silty loam corresponding to the lowest conductivity and polarization values, and (2) at the bottom a lignite layer corresponding to the highest conductivity (σ'= 60 mS/m) but low polarization (σ''< 0.25 mS/m) values. While no groundwater was observed during the drilling of B1 and B2, the recovered sediments were often close to saturation in the loamy soils (see Appendix 5.4). The high σ' values are interpreted as being caused by the contribution of both surface and electrolytic conduction. Due to the fine texture of clays, polarization is mainly expected at frequencies above > 10 Hz, explaining the low σ'' values at 1 Hz (see e.g., Mendieta et al.,2021). The increase in both σ' and σ'' for the lignite at depths below 7 m is expected due to the high surface charge of organic soils, which contributes to interfacial conductivity and polarization (e.g., Shao et al., 2017; Gao et al., 2017; Katona et al., 2021). A clear anomaly is also revealed in the loamy soils associated to the highest polarization values (σ''> 0.5 mS/m) in the profile. The anomaly is located below 2m depth, so unlikely to be related to infrastructure, yet above the expected position of the lignite layer.

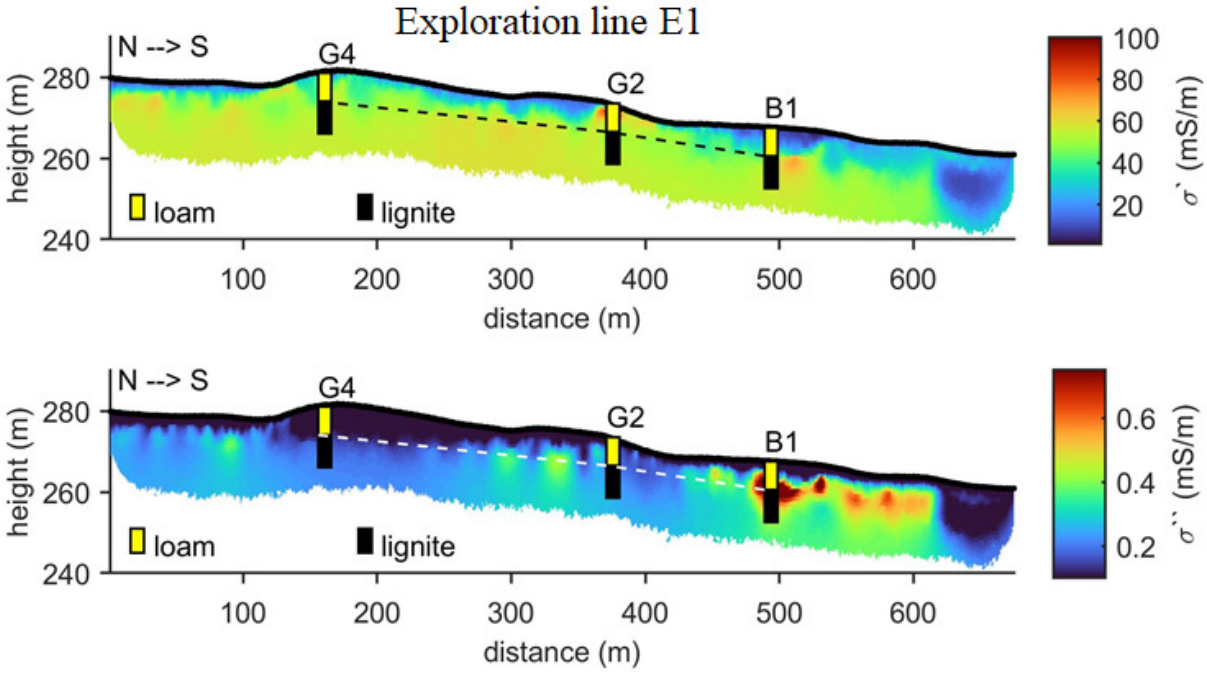

Figure 1: CC imaging results obtained for the Exploration line E1, expressed in terms of the conductivity (σ') and polarization (σ''). The information about lithological changes observed in soil samples extracted from existing boreholes G4 and G2, as well as the drilled borehole for this study (B1), is imposed on the electrical images for comparison. The dashed line represents the depth to the lignite layer from the linear interpolation of the borehole data.

Figure 2 shows the imaging results for parallel line SIP1 for data collected at different frequencies. Overall, the values are consistent to those in E1. The shape of the shallow polarizable anomaly is clearly resolved between 2 and 6 m depth at the middle of the SIP1 profile, with the highest polarization (σ'' ~ 1 mS/m) at low frequencies (0.5 and 1 Hz) and a negligible response at frequencies above 7.5 Hz. In contrast, the conductivity images reveal only a layered media and no variation at the position of the polarization anomaly. Figure 2 reveals vertical changes in σ' consistent with those observed in cores from B1 and B2, with lower values (~20 mS/m) for sandy loam than for the clayey loam. Figure 2 also shows a shallow conductivity anomaly (between 10 and 20 m profile distance), which is only polarizable at frequencies above 10 Hz, likely indicating the presence of clay-rich sediments. The frequency at which the maximum polarization is observed is inversely proportional to grain size (see Bücker et al., 2019), and laboratory results have reported the maximum response in clays at frequencies between 10 - 100 Hz (see Mendieta et al., 2021 and references therein) supporting the interpretation of the conductive and polarizable shallow anomaly observed between 10 and 20 m along the SIP1 profile.

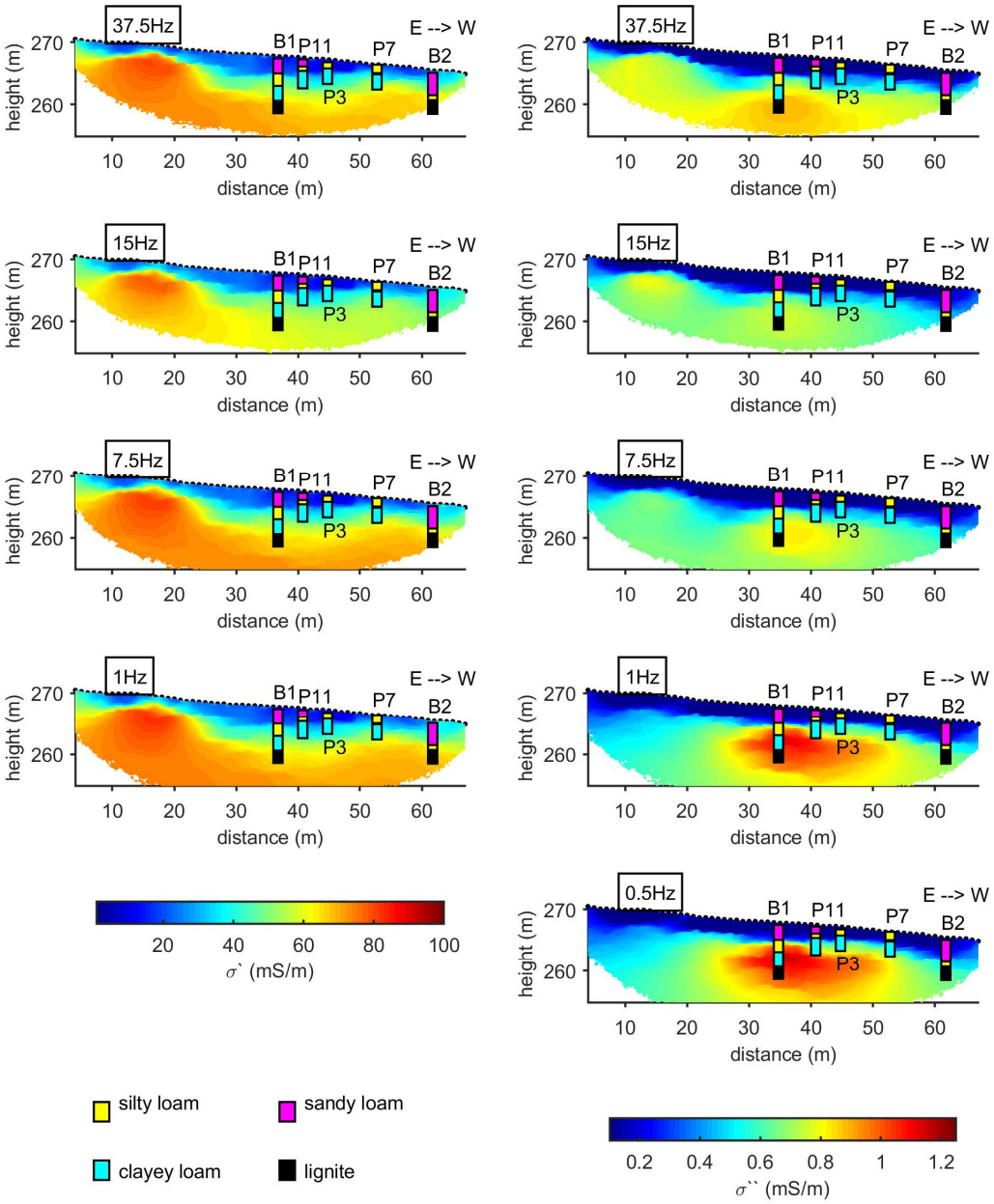

Figure 2: CC imaging results obtained for multi-frequency data collected at the line SIP1 expressed in terms of the conductivity (σ') and polarization (σ''). The information about lithological changes observed in soil samples extracted from existing piezometers (P11 and P7), as well as the drilled boreholes for this study (B1 and B1) is imposed on the electrical images for comparison.

2.2 The deep carbon stock: geochemical interpretation of the high electrical polarization anomaly

Figure 3 shows the chemical and physical analysis of the soil samples from B1 and B2 and the vertical conductivity (σ') and polarization (σ'') values extracted from the SIP1 data at the position of the boreholes. Such plots demonstrate the highest σ'' values are resolved at 1 Hz in B1 between 2 and 6 m depth. The σ'' values of B1 are almost twice those of B2, although the clay content is 50% lower; thus, the polarization anomaly cannot be explained by changes in the textural properties of soil, especially at low frequencies. The surface charge, as indicated by the CEC, is consistent in both boreholes, with the lowest values in the loam soils and an abrupt increase at the position of the lignite layer.

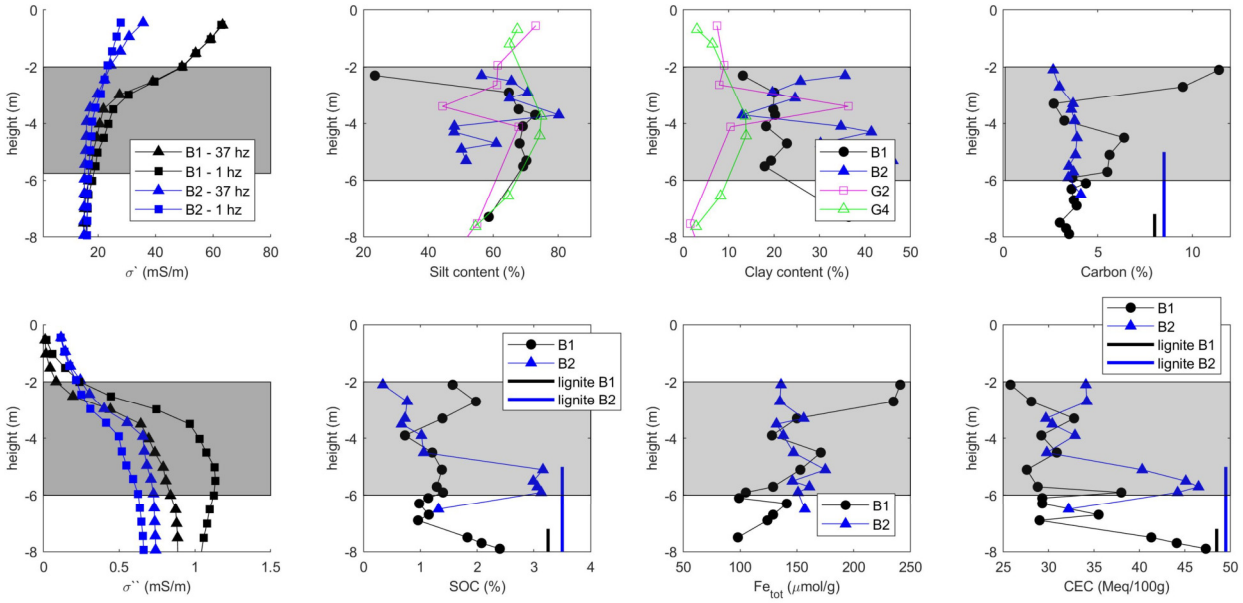

Figure 3: Comparison of the electrical (σ' and σ'') and geochemical parameters (Fe_{tot}, TOC, CEC) measured in the drilling cores (B1 and B2). Electrical parameters represent the mean values computed from pixels extracted from the inversion results of lines SIP1 at 1 Hz (solid triangles) and 37.5 Hz (solid circumferences). Textural properties in boreholes (B1 and B2) and piezometer samples are also presented for comparison. The depth to the lignite layer found at the position of B1 and B2 is indicated by the vertical lines in the plots of the SOC, Carbon and CEC data.

The polarizable anomaly ($\sigma'' > 1$ mS/m) at B1 is collocated with the highest SOC (> 1%) and Fe_{tot} concentrations. In comparison, geoelectrical and geochemical parameters are both much lower in B2. It might be argued that the increase in iron content enhances the electrode polarization observed in iron sulfides. However, XRD scans in our samples revealed negligible concentrations of sulfides, with the mineralogy being dominated by calcite and silicates. Hence, iron is mainly present as iron oxides, commonly related to negligible polarization at 1 Hz, with the exception of Hematite (e.g., Hubbard et al., 2014; Abdel Aal, 2014), which was also not found in our samples neither in soils nor bound to organic matter.

The polarizable anomaly is most likely related to two organic carbon rich layers: (1) the main one found between 2 and 3 m depth (> 2 % SOC), and (2) a deeper stock between 4 and 6 m depth (ca 1.5 % SOC). This interpretation is supported by the geochemical analysis of sediments in B1. High σ'' and SOC in B2 at 5 m depth are due to the presence of the lignite layer, which is observed at 7.2 m depth in B1.

3 Discussions

Results presented above demonstrate that soil textural properties of the HOAL vary enormously in space, making a reliable characterization from a few discrete soil samples difficult. Moreover, CC imaging results for E1 and SIP1 reveal a distinctive polarizable anomaly (σ''>0.6 mS/m) within 3 m and 6 m depth. At the HOAL, this is the only location at which such high polarization values have been observed. Analysis of samples collected in B1 and B2 demonstrate this anomaly is not due to buried infrastructure (pipes, cables etc) or changes in clay content, yet variations in σ'' are consistent with changes in SOC and Fe_{tot} concentrations supporting our interpretation of deep carbon stocks. The SOC concentrations observed in these deep carbon stocks are similar to the value (~2.1 %) in Austrian topsoils, as reported by Panagos et al. (2013).

Mineralization of C is higher in coarse-textured soils (e.g., Hassnik, 1992), with finer grains hindering the access of soil microbes and O_2 to the SOC. Additionally, clay and iron oxide surfaces adsorb C, forming soil aggregates that protect SOC from decomposition (Elliot, 1986). Hence, low permeable loams from the HOAL offer the best conditions to preserve SOC from O_2, which could trigger its decomposition. The carbon stocks found are supported by the presence of iron oxides (as reported by high Fe_{tot} concentrations) which contribute to the sorption and stabilization of SOC (see Singh et al., 2018 and references therein).

Our results are consistent with those recently reported by Peshtani et al. (2025), who reported an increase in σ' and σ'' following the adsorption of pentaglycine into the surface of ferrihydrite-coated sand and ceramic beads. The increase in the polarization (σ'') is explained by electrostatic and chemical interactions between the reactive mineral surface and functional groups present in the organic matter such as amine and carboxyl.

Our results are also consistent with previous studies revealing an increase in the polarization with increasing carbon concentration in peatlands (McAnallen et al., 2018; Katona et al., 2021; Strobel et al., 2023) and in municipal solid waste (Flores Orozco et al., 2020). Gao et al. (2017; 2019) have also found evidence for the sensitivity of the method to organic carbon in biochar measurements. Though further research is needed to quantitatively resolve SOC-CC associations or, as also pointed out by Peshtani et al. (2025), identify the nature of the organo-mineral complexes.

Our results demonstrate that the CC method may help to overcome the limitations in SOC investigations based solely on a few soil samples. However, interpreting CC results still requires boreholes soil data as ground truthing. Hence, we believe that CC would be a useful tool when designing the soil sampling campaigns. For our study, chemical analysis of samples allowed us to differentiate between two separated carbon stocks revealed by the polarizable anomaly in the CC images. Since the geochemical and geophysical measurements represent very different sampling volumes (a few grams in the soil analysis vs. a few m^3 in the geophysical data), we refrained from a quantitative estimation of SOC from σ'' values. Nonetheless, volume

estimates of SOC can be obtained from 3D electrical models of geophysical data as presented in the Appendix A5.5 (Figure A2). Further investigations should consider CC laboratory and field monitoring experiments to understand organic carbon dynamics, such as sequestration and degradation of SOC.

4 Conclusions

We present a novel application of electrical geophysical methods to resolve variations in soil organic carbon (SOC) in an imaging framework. Our results demonstrate the potential of the complex conductivity imaging method to map carbon stocks in soils in a depth between 4 and 6 m. Electrical anomalies with high polarization (i.e., capacitive properties) at frequencies $\leq$ 1 Hz indicate high SOC, a feature not resolved by the electrical conductivity, which is highly sensitive to lithological variations. While support of soil analysis is necessary for a quantitative interpretation of electrical properties, our study demonstrates the advantages of using the CC method to select the position of drilling for soil sampling. Hence, CC may provide a unique opportunity to investigate deep carbon storage, for instance in thawing arctic soils, as well as to understand the temporal dynamics of SOC.

5 Appendix

5.1 The Hydrological Open Air Laboratory (HOAL)

All data sets were collected at the HOAL, located in Petzenkirchen (Austria), which is a 66 ha observatory dedicated to understanding water-related flow and transport processes involving sediments, nutrients and microbes in small catchments (Blöschl et al., 2016). Soil cores recovered from eight boreholes distributed across the HOAL (G1 to G8 in Figure A1) reveal only silty loam soils underlain by a succession of consolidated and unconsolidated lignite. Topography variations (see Figure A1) are aligned with variations in the depth to the lignite layer between 6 m and 40 m. The silty loam soils exhibit low saturated hydraulic conductivity (< 10^{-7} m s^{-1}) and may give rise to discrete perched aquifers, while an artesian aquifer was found below the consolidated lignite. Further details about the site can be found in Blöschl et al. (2016).

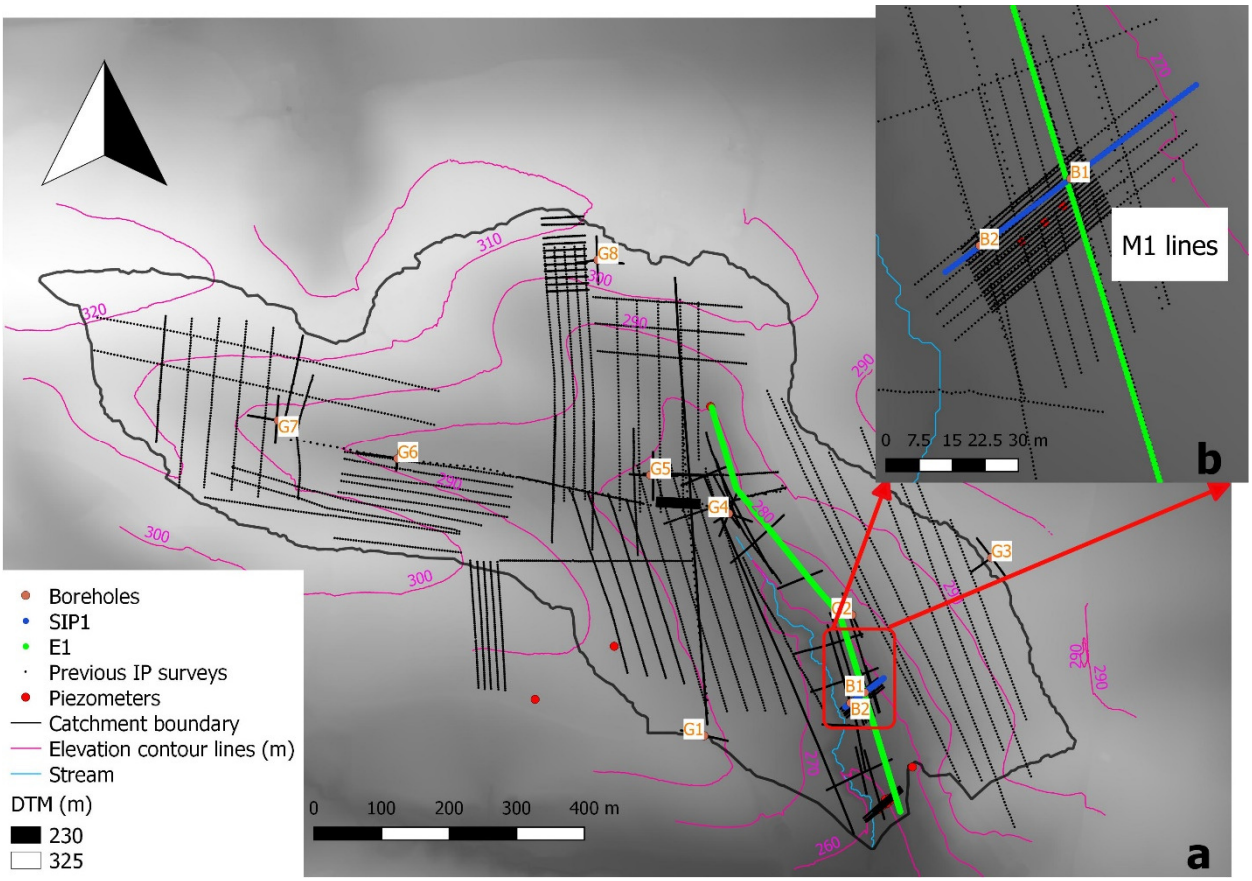

Figure A1: Existing surface and subsurface information at the HOAL: (1a) The topography changes are indicated in the grey tones and the isolines (pink lines), available CC measurements (black lines) and boreholes (G1 to G8). The embedded plot (1b) highlights the orientation of the CC lines presented in this study: exploration results (E1 with the green line), the multi-frequency measurements (SIP1 with the blue line) and mapping measurements (M1 indicated with the black lines) as well as the boreholes B1 and B2 drilled for sampling and geochemical analysis of soil samples in the electrical anomaly.

5.2 The Complex Conductivity Imaging method

The complex conductivity (CC) method is also known as complex resistivity (CR), electrical impedance tomography or induced polarization (IP). The method uses a pair of electrodes to impose an electrical field into the ground (i.e., related to current flow), while another pair of electrodes measures the resulting voltage. Imaging methods deploy tens to hundreds of electrodes, where thousands of measurements can be used to compute spatial changes in the electrical properties of the subsurface. The method operates at frequencies below 10 kHz, where the electrical properties of the soil are due to the movement of free charges in the pore water (electrolytic conduction), in the EDL formed at the grain-fluid interface (interfacial or surface conductivity) or through the solid particle of the soil (matrix conduction). In the absence of electronic conductors and semi-conductors, the matrix conduction is negligible; thus, the electrical conductivity of the soils is given by electrolytic (σ_{el}) and surface conductivity (σ_s). While σ_{el} is controlled by the saturation, porosity and conductivity of the fluid; the σ_s is mainly controlled by the surface area and surface charge in the EDL. Moreover, the application of an external field results in the polarization of charges in the EDL. Accordingly, the surface conductivity is represented as a complex value (σ^*) contributing to bulk conductivity (σ_s') and the so-called polarization effect (σ_s''). Hence, the low-frequency properties of the soil can be expressed by means of the complex conductivity, such as:

$$\sigma^* = \sigma' + i\sigma'' = (\sigma_{el} + \sigma_s') + i\sigma_s' \quad (1)$$

In Eq. 1, i represents the imaginary unit ($i^2 = -1$).

The CC can use direct-current (DC) or alternating-current (AC), with the former referred to as time-domain (TD) and the latter as frequency-domain (FD). In the FD, the polarization effect results in a phase-shift between the sinusoidal current imposed in the current dipole and the voltage measured; whereas in the TD, the polarization effect results in a decaying secondary electrical field observed after switching the current off. In the FD, it is common to use currents in the range between 0.1 mHz and 10 kHz; while in the TD it is common to use a square wave with a pulse-length varying between 0.2 and 8 s. For further details see Ward, 1980, Binley and Kemna (2005), Sumner (2012), Binley and Slater (2020).

The resolution of the CC method is controlled by the separation between the electrodes used for the voltage measurements; while the depth of investigation is defined by the maximum separation between the transmitting dipole (i.e., dipole used to inject current) and the voltage dipole. However, increasing the separation between current and voltage dipole also decreases the signal-to-noise ratio (S/N). To increase the S/N, it is necessary to increase the dipole length. Hence, geophysical surveys need to be carefully designed to achieve a high resolution (enhanced by decreasing the dipole lengths) and reach the required depth of investigation (enhanced by increasing the dipole length). It is well accepted that the maximal resolution in the CC imaging results is given by 1/3 of the dipole length, while the depth of investigation is approximately 1/3 of the maximum separation for the current and voltage dipole. However, the presence of highly conductive materials (e.g., clay-rich soils) close to the surface might channel current flow reducing the depth of investigation. We refer to Sasaki, 1992; Friedel, 2003; Okpoli, 2013.

Kemna (2000) demonstrated that the resolution of the CC imaging results can be evaluated by means of the cumulative sensitivity. In electrical imaging, sensitivity quantifies the effect that changes in the electrical properties at a given position of the imaging plane (i.e., model parameter) have on the measured voltages at the surface (Kemna, et al., 2002). Accordingly, high sensitivity is resolved for measurements with small separation between current and voltage dipoles (i.e., close to the surface) and it gradually decreases at depth. The sensitivity for each model parameter of the electrical image (i.e., volume for 3D measurements) is calculated within the inversion, whereas the cumulative sensitivity for each model parameter is the sum of the values calculated for each current injection in an imaging data set (i.e., 4-electrode arrays). The cumulative sensitivity is commonly expressed as a normalized value (i.e., divided by the highest sensitivity value found in a given imaging data set) on a logarithm scale. Accordingly, low cumulative sensitivity values can be used to exclude poorly resolved areas in the imaging plane (i.e., volume for 3D measurements). We refer to Kemna, 2000 and Weigand et al. (2017) for further details.

5.3 Collection and processing of the CC data presented in this study

The CC measurements presented here were carried out with the DAS-1 instrument (Multiphase Technology, MPT) using coaxial cables to reduce distortions in the data by electromagnetic (EM) coupling (Flores Orozco et al., 2021). More than 150 lines CC have been collected in the HOAL. In this study, we present only imaging results for three data sets: M1, E1, and SIP1. E1 refers to an exploration line collected at 1 Hz using a roll-along scheme for a total of 676 electrodes and 1 m spacing between them. The SIP1 line was collected perpendicular to E1, with 64 electrodes (1 m spacing) with 10 frequencies between 0.5 and 225 Hz to gain information about the frequency-dependence of the electrical properties. The mapping data M1 comprises 27 lines using 72 electrodes in each line (further details in Appendix A.5.5). The position and orientation of the lines is indicated in Figure A1.

All CC measurements were collected using a dipole-dipole skip-0 configuration (i.e., the dipole length is the same as the electrode spacing) and all possible skip-0 dipoles. The configuration conducted voltage measurements always ahead of the current dipole to minimize contamination of the data due to enhanced redox reactions in the electrodes used to inject current (i.e., polarization of the electrodes). Measurements were collected as normal and reciprocals (i.e., interchanging the current and voltage dipoles). Erroneous measurements filtered in all data correspond to those quadrupoles associated to negative resistances and apparent resistivity readings (after modelling the numerical geometric factor for each quadrupole) as well as those measurements where normal and reciprocal pairs deviate over 75% their mean value. Normal and reciprocal misfit analysis was conducted in representative measurements to quantify data error (see Flores Orozco et al., 2012b, 2021; 2022). Moreover, for data collected at different frequencies, we deleted those measurements (i.e., 4-electrode arrays) not found in all frequencies under investigations. This ensures a consistent sensitivity in all CC imaging across the different frequencies. We used CRTomo (Kemna, 2000) for the inversion of the data. Inversion results are presented in terms of real and imaginary components of the complex conductivity.

The highest resolution in our SIP investigations (c.f., Figure 2 and Figure 3) is 0.35 cm, corresponding to 1/3 of the dipole length. Such resolution is found close to the surface, with numerical simulations revealing that a polarizable anomaly ($\sigma'' = 1$ mS/m, such as the one observed in Figure 2) can be resolved to a maximum depth 7 m but is not detected below such depth. The maximum separation between current and voltage dipoles is 29 m, corresponding to a nominal depth of investigation of 9.7 m. In the analysis of the CC inversion results, all model parameters with a logarithmic cumulative sensitivity below -3 were excluded. This has been demonstrated to be an appropriate threshold for identifying the reliable data in CC imaging results as shown by Weigand et al. (2017). Nonetheless, numerical simulations were performed in this study to validate the selected threshold.

5.4 Ground truth: analysis of borehole sediments

During the field surveys, two boreholes (B1 and B2 in Figure A1) were drilled to a depth of 8 m for the collection of soil samples. Soils were immediately packed in dry ice to avoid chemical transformations during transport and storage. Soil chemical analysis was performed after the samples were freeze-dried and milled using an agate ball mill. Total carbon was measured by combustion using a Thermo Quest CN element analyser at the Bayreuth Keylab for Experimental Biogeochemistry. Reactive iron (Fe_{tot}) was classified as the total Fe concentration in samples after extraction by 1M HCl after 24h on a horizontal shaker. The extract was filtered (0.45 µm) and analysed for total Fe photometrically using the phenanthroline method (Wallmann et al., 1993; Tamura et al., 1974). The cation exchange capacity (CEC) was determined with an ICP-OES after Matschonat and Matzner (1995), except that Fe and Mn were also included in the CEC calculation in addition to the base cations. The inorganic carbon content was measured using the method described by Horváth et al., (2005) with replicate RSDs of core samples ranging from 0.8 to 2 %. The SOC carbon content is the total carbon minus inorganic carbon content. Grain sizes of sediments obtained in B1 and B2, as well as from previously drilled boreholes G2, and G4, and from four piezometers (see Figure A1) were measured by sieve analysis. Groundwater electrical conductivity (EC) measured in the piezometers was about 40 mS/m during the measurement campaign.

5.5 The geometry of the deep carbon stock

Figure A2 shows the extension of the polarization (σ'') anomaly resolved at 4 m depth as obtained from the interpolation of the complex conductivity imaging results from the inversion of all mapping lines referred to as M1. The mapping M1 consists of 32 lines, namely: 5 long and 17 short lines parallel to the stream direction (roughly N-S), as well as 5 long and 5 short lines perpendicular to them (roughly W-E). Long lines have a separation of 5 m between them and were carried out using 72 electrodes in each, with 1 m spacing between electrodes, whereas short lines have 1 m separation between them, each with 72

electrodes and a spacing of 0.5 m. The data were inverted for each independent line using CRTomo using the same methodology as the one used for the processing and inversion of lines E1 an SIP1 (see A5.3). Nonetheless, the 3D inversion of all M1 lines was also conducted with other inversion algorithms in actual 3D (data not shown) revealing consistent results with the Figure A2 presented below. Considering that the data was collected independently for each electrode line, we decided here to work only with 2D inversion.

The geometry of the carbon stock at 4 m depth presented in A2 corresponds to the high polarization values (σ``> 900 μS/m) extracted from the inversion of the M1 data. These values are consistent to those observed in the E1 and SIP lines (Figure 2 and 3). The map presented in Figure A2 reveals that the carbon stock extends towards the northwest from the drilled boreholes B1, where the high organic carbon content was measured in soil samples (Figure 4). The map presented in Figure A2 can be used to guide further drilling for the collection of soil samples.

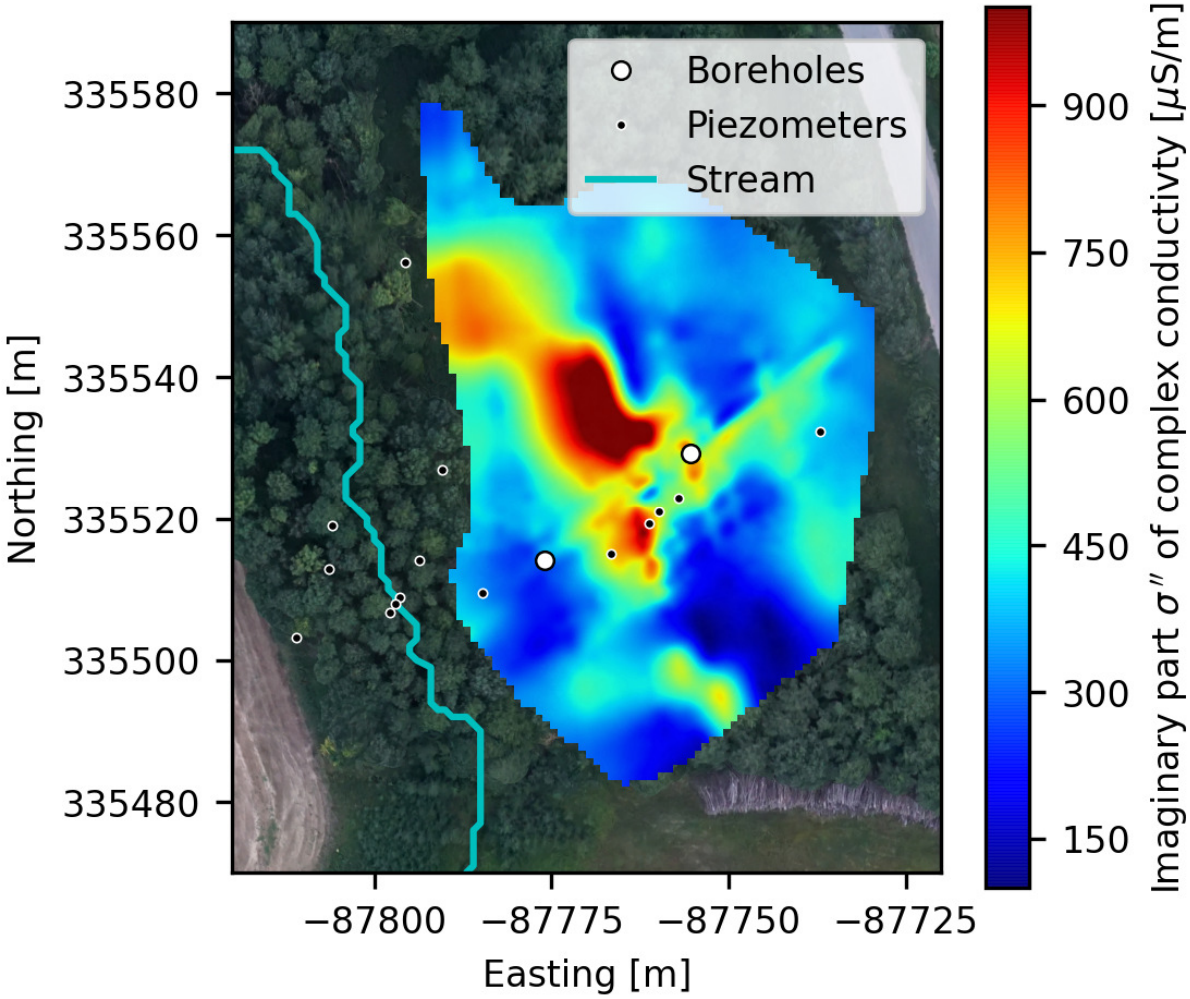

Figure A2. Geometry of the deep carbon stock (at 4 m depth) given by the anomalous high induced polarization values (σ'' > 1 mS/m)

6 Data availability

Data presented here are available at the repository of the TU Wien with the digital object identifier (DOI): https://doi.org/10.48436/5h7jb-26w42

7 Author contribution

AFO designed the experiments, while JG and TK carried out field data, with laboratory analysis of samples conducted by BG. AFO conducted the Data Curation, Formal Analysis, Methodology and Visualization. AFO, GB, PS and SF were in charge of Resources. AFO prepared the manuscript with contributions from all co-authors.

References

Abdel Aal, G.Z., Atekwana, E.A. & Revil, A. 2014. Geophysical signatures of disseminated iron minerals: A proxy for understanding subsurface biophysicochemical processes. Journal of Geophysical Research: Biogeosciences, 119(9), pp.1831-1849.

Atekwana, E.A. and Slater, L.D., 2009. Biogeophysics: A new frontier in Earth science research. Reviews of Geophysics, 47(4).

Bernal, B., Megonigal, J.P. and Mozdzer, T.J., 2017. An invasive wetland grass primes deep soil carbon pools. *Global Change Biology*, *23*(5), pp.2104-2116.

Binley, A., Hubbard, S.S., Huisman, J.A., Revil, A., Robinson, D.A., Singha, K. & Slater, L.D. 2015. The emergence of hydrogeophysics for improved understanding of subsurface processes over multiple scales. Water resources research, 51(6), pp.3837-3866.

Binley, A. and Kemna, A., 2005. DC resistivity and induced polarization methods. In *Hydrogeophysics* (pp. 129-156). Dordrecht: Springer Netherlands.

Blöschl, G., A. P. Blaschke, M. Broer, C. Bucher, G. Carr, X. Chen, A. Eder, M. Exner-Kittridge, A. Farnleitner, A. Flores-Orozco, P. Haas, P. Hogan, A. Kazemi Amiri, M. Oismüller, J. Parajka, R. Silasari, P. Stadler, P. Strauß, M. Vreugdenhil, W. Wagner and M. Zessner (2016) The Hydrological Open Air Laboratory (HOAL) in Petzenkirchen: a hypothesis-driven observatory, Hydrology and Earth System Sciences, 20, 227-255, doi:10.5194/hess-20-227-2016.

Binley, A. and Slater, L., 2020. *Resistivity and induced polarization: Theory and applications to the near-surface earth*. Cambridge University Press.

Button, E.S., Pett-Ridge, J., Murphy, D.V., Kuzyakov, Y., Chadwick, D.R. & Jones, D.L. (2022). Deep-C storage: Biological, chemical and physical strategies to enhance carbon stocks in agricultural subsoils. Soil Biology and Biochemistry, 170, p.108697.

Elliott, E., 1986. Aggregate structure and carbon, nitrogen, and phosphorus in native and cultivated soils. Soil science society of America journal, 50(3), pp.627-633.

Flores Orozco, A., Williams, K.H., Long, P.E., Hubbard, S.S. and Kemna, A., 2011. Using complex resistivity imaging to infer biogeochemical processes associated with bioremediation of an uranium-contaminated aquifer. Journal of Geophysical Research: Biogeosciences, 116(G3).

Flores Orozco, A., Williams, K.H. and Kemna, A., 2013. Time-lapse spectral induced polarization imaging of stimulated uranium bioremediation. Near Surface Geophysics, 11(5), pp.531-544.

Flores-Orozco, A., Gallistl, J., Steiner, M., Brandstätter, C. and Fellner, J., 2020. Mapping biogeochemically active zones in landfills with induced polarization imaging: The Heferlbach landfill. Waste Management, 107, pp.121-132.

Flores Orozco, A., Micić, V., Bücker, M., Gallistl, J., Hofmann, T. and Nguyen, F., 2019. Complex-conductivity monitoring to delineate aquifer pore clogging during nanoparticles injection. Geophysical Journal International, 218(3), pp.1838-1852.

Flores Orozco, A., Velimirovic, M., Tosco, T., Kemna, A., Sapion, H., Klaas, N., Sethi, R. and Bastiaens, L., 2015. Monitoring the injection of microscale zerovalent iron particles for groundwater remediation by means of complex electrical conductivity imaging. Environmental science & technology, 49(9), pp.5593-5600.

Friedel, S., 2003. Resolution, stability and efficiency of resistivity tomography estimated from a generalized inverse approach. *Geophysical Journal International*, *153*(2), pp.305-316.

Ganzenmüller, R., Obermeier, W.A., Bultan, S., Spawn-Lee, S.A., Zabel, F. and Pongratz, J., 2025. Humans have depleted global terrestrial carbon stocks by a quarter. *One Earth*, *8*(8).

Gao, Z., Haegel, F.H., Huisman, J.A., Esser, O., Zimmermann, E. and Vereecken, H., 2017. Spectral induced polarization for the characterisation of biochar in sand, Near surface geophysics, 15(6), pp.645-656.

Gao, Z., Haegel, F.H., Esser, O., Zimmermann, E., Vereecken, H. and Huisman, J.A., 2019. Spectral induced polarization of biochar in variably saturated soil, Vadose zone journal, 18(1), pp.1-13.

Harper, R.J. and Tibbett, M., 2013. The hidden organic carbon in deep mineral soils. *Plant and Soil*, *368*(1), pp.641-648.

Harrison, R.B., Footen, P.W. and Strahm, B.D., 2011. Deep soil horizons: contribution and importance to soil carbon pools and in assessing whole-ecosystem response to management and global change. *Forest Science*, *57*(1), pp.67-76.

Hassink, J., 1992. Effects of soil texture and structure on carbon and nitrogen mineralization in grassland soils, Biology and Fertility of Soils, 14, pp.126-134.

Horváth, B., Opara-Nadi, O. and Beese, F., 2005. A simple method for measuring the carbonate content of soils, Soil Sci. Soc. Am. J., 69: 1066-1068. doi.org/10.2136/sssaj2004.0010

Hubbard, C.G., West, L.J., Rodriguez-Blanco, J.D. and Shaw, S., 2014. Laboratory study of spectral induced polarization responses of magnetite—Fe 2+ redox reactions in porous media, Geophysics, 79(1), pp.D21-D30.

Johansson, S., Fiandaca, G., and Dahlin, T.: Influence of non-aqueous phase liquid configuration on induced polarization parameters: Conceptual models applied to a time-domain field case study, Journal of Applied Geophysics 123 (2015): 295-309.

Katona, T., Gilfedder, B.S., Frei, S., Bücker, M. and Flores-Orozco, A., 2021. High-resolution induced polarization imaging of biogeochemical carbon turnover hotspots in a peatland, Biogeosciences, 18(13), pp.4039-4058.

Kemna, A., 2000. *Tomographic inversion of complex resistivity: Theory and application*. Der Andere Verlag.

Kemna, A., Vanderborght, J., Kulessa, B. and Vereecken, H., 2002. Imaging and characterisation of subsurface solute transport using electrical resistivity tomography (ERT) and equivalent transport models. *Journal of hydrology*, *267*(3-4), pp.125-146.

Kessouri, P., Furman, A., Huisman, J.A., Martin, T., Mellage, A., Ntarlagiannis, D., Bücker, M., Ehosioke, S., Fernandez, P., Flores-Orozco, A. and Kemna, A., 2019. Induced polarization applied to biogeophysics: recent advances and future prospects. *Near Surface Geophysics*, *17*(6-Recent Developments in Induced Polarization), pp.595-621.

Matschonat, G. and Matzner, E., 1995. Quantification of ammonium sorption in acid forest soils by sorption isotherms. *Plant and Soil*, *168*(1), pp.95-101.

Mendieta, A., Jougnot, D., Leroy, P. and Maineult, A., 2021. Spectral induced polarization characterization of non-consolidated clays for varying salinities—An experimental study, Journal of Geophysical Research: Solid Earth, 126(4), p.e2020JB021125.

McAnallen, L., Doherty, R., Donohue, S., Kirmizakis, P. and Mendonça, C., 2018. Combined use of geophysical and geochemical methods to assess areas of active, degrading and restored blanket bog, Science of the Total Environment, 621, pp.762-771.

Mellage, A., Zakai, G., Efrati, B., Pagel, H. and Schwartz, N., 2022. Paraquat sorption-and organic matter-induced modifications of soil spectral induced polarization (SIP) signals. *Geophysical Journal International*, *229*(2), pp.1422-1433.

Ntarlagiannis, D., Williams, K.H., Slater, L. and Hubbard, S., 2005. Low-frequency electrical response to microbial induced sulfide precipitation, Journal of Geophysical Research: Biogeosciences, 110(G2).

Okpoli, C.C., 2013. Sensitivity and resolution capacity of electrode configurations. *International Journal of Geophysics*, *2013*(1), p.608037.

Panagos, P., Hiederer, R., Van Liedekerke, M. and Bampa, F., 2013. Estimating soil organic carbon in Europe based on data collected through an European network, Ecological Indicators, 24, pp.439-450.

Peshtani, K., Robinson, J., Torgeson, J., Rabideaux, N., Slater, L. and Qafoku, N.P., 2025. Investigating soil organic matter complexation in natural analog systems using geoelectrical methods. *Environmental Science & Technology*, *59*(34), pp.18203-18212.

Ponziani, M., Slob, E.C., Vanhala, H. and Ngan-Tillard, D.J.M., 2012. Influence of physical and chemical properties on the low-frequency complex conductivity of peat, Near Surface Geophysics, 10(6), pp.491-501.

Sasaki, Y., 1992. Resolution of resistivity tomography inferred from numerical SIMULATION1. *Geophysical prospecting*, *40*(4), pp.453-463.

Schwartz, N. and Furman, A., 2012. Spectral induced polarization signature of soil contaminated by organic pollutant: Experiment and modelling, Journal of Geophysical Research: Solid Earth, 117(B10).

Shao, Z., Revil, A., Mao, D. and Wang, D., 2017. Induced polarization signature of coal seam fires, Geophysical Journal International, 208(3), pp.1313-1331.

Seigel, H., Nabighian, M., Parasnis, D.S. and Vozoff, K., 2007. The early history of the induced polarization method, The Leading Edge, 26(3), pp.312-321.

Singh, M., Sarkar, B., Sarkar, S., Churchman, J., Bolan, N., Mandal, S., Menon, M., Purakayastha, T.J. and Beerling, D.J., 2018. Stabilization of soil organic carbon as influenced by clay mineralogy, Advances in agronomy, 148, pp.33-84.

Sumner, J.S., 2012. *Principles of induced polarization for geophysical exploration* (Vol. 5). Elsevier.

Strauss, J., Schirrmeister, L., Grosse, G., Wetterich, S., Ulrich, M., Herzschuh, U. and Hubberten, H.W., 2013. The deep permafrost carbon pool of the Yedoma region in Siberia and Alaska. *Geophysical Research Letters*, *40*(23), pp.6165-6170.

Strobel, C., Dörrich, M., Stieff, E.H., Huisman, J.A., Cirpka, O.A. and Mellage, A., 2023. Organic matter matters—The imaginary conductivity of sediments rich in solid organic carbon, Geophysical Research Letters, 50(23), p.e 2023GL104630.

Tamura, H., Goto, K., Yotsuyanagi, T., and Nagayama, M., 1974. Spectrophotometric determination of iron (II) with 1, 10phenanthroline in the presence of large amounts of iron (III). Talanta, 21, 314–318

Tarnocai, C., Canadell, J.G., Schuur, E.A., Kuhry, P., Mazhitova, G. and Zimov, S., 2009. Soil organic carbon pools in the northern circumpolar permafrost region. *Global biogeochemical cycles*, *23*(2).

Walter Anthony, K., Schneider von Deimling, T., Nitze, I., Frolking, S., Emond, A., Daanen, R., Anthony, P., Lindgren, P., Jones, B. and Grosse, G., 2018. 21st-century modeled permafrost carbon emissions accelerated by abrupt thaw beneath lakes. *Nature communications*, *9*(1), p.3262.

Ward, S.H., 1980. Electrical, electromagnetic, and magnetotelluric methods. *Geophysics*, *45*(11), pp.1659-1666.

Wallmann, K., Hennies, K., König, I., Petersen, W., and Knauth, H.D., 1993. New procedure for determining reactive Fe(III) and Fe(II) minerals in sediments, Limnology and Oceanography, 38.

Wainwright, H.M., Flores Orozco, A., Bücker, M., Dafflon, B., Chen, J., Hubbard, S.S. and Williams, K.H., 2016. Hierarchical Bayesian method for mapping biogeochemical hot spots using induced polarization imaging, Water Resources Research, 52(1), pp.533-551.

Weigand, M., Orozco, A.F. and Kemna, A., 2017. Reconstruction quality of SIP parameters in multi-frequency complex resistivity imaging. *Near Surface Geophysics*, *15*(2), pp.187-199.

Williams, K.H., Ntarlagiannis, D., Slater, L.D., Dohnalkova, A., Hubbard, S.S. and Banfield, J.F., 2005. Geophysical imaging of stimulated microbial biomineralization. *Environmental science & technology*, *39*(19), pp.7592-7600. Yost, J.L. and Hartemink, A.E., 2020. How deep is the soil studied–an analysis of four soil science journals. Plant and soil, 452, pp.5-18.